A Diagnostic Study of Atmospheric Spectral Kinetic Energetics

WILLIAM R. BURROWS

Atmospheric Environment Service, Environment Canada, Downsview, Ontario M3H 5T4

(Manuscript received 2 October 1975, in revised form 8 April 1976)

ABSTRACT

Wind spectra are obtained from data using expansions in spherical harmonics. Equations governing the tendencies of total kinetic energy of the spectral wind components are derived. Dissipation is obtained diagnostically as a residual. Calculations are performed on a data set for two weeks at eight pressure levels from surface to 100 mb for the Northern Hemisphere. As the data coverage is not global, parity assumptions are necessary for scalar data fields and are assigned based on observation and the geostrophic wind equations. Results are scaled by the two-dimensional index n (degree of associated Legendre functions P_n^l). Expansions are truncated at $l=n=24$. Data accuracy may be questionable for the higher coefficients considered here.

Some of the results of calculations are as follows:

1) Kinetic energy above 850 mb is maximum in scales $n=2$ and 4, with a secondary maximum at $n=9$. Equipartition of u and v kinetic energy occurs at $n=7$.

2) Dissipation residuals are large in every scale, suggesting large fluxes of kinetic energy between scales $n>24$ and $n\leqslant 24$.

3) The total nonlinear horizontal transfer of kinetic energy shows sources in scales $4\leqslant n\leqslant 10$, $13\leqslant n\leqslant 15$, $n=18$ and $n=23$, with strongest sources in scales $n=7$ and 9. The source at $n=18$ is isolated and strong and may be due to the ITCZ. Scales $n\leqslant 3$ gain kinetic energy in the fashion of the familiar zonal flow in calculations where data are expanded in Fourier series at latitude circles.

4) The presence of sources of kinetic energy in scales $15\leqslant n\leqslant 24$, and the fact that slopes of kinetic energy with scale are generally not close to -3, suggest these scales do not form an inertial subrange.

5) The contributions of interactions of scales $0\leqslant n\leqslant 6$, $7\leqslant n\leqslant 14$ and $15\leqslant n\leqslant 24$ to the total nonlinear horizontal transfer of kinetic energy in each scale $0\leqslant n\leqslant 24$ were isolated, and the method is suggested as a means of diagnosing the impact of dissipation and heating parameterizations upon all scales of motion in models of the atmosphere. Interactions involving scales $7\leqslant n\leqslant 14$ are quite active, and those involving scales $15\leqslant n\leqslant 24$ are surprisingly active in view of their small kinetic energy content. Self-interactions in the latter scale range transfer a great deal of kinetic energy into ultra-long scales ($n\leqslant 3$) and out of $n=4$ in the upper troposphere, while self-interactions in the $7\leqslant n\leqslant 14$ scale range (scale of baroclinic mid-latitude disturbances) transfer much of the kinetic energy out of scales $4\leqslant n\leqslant 9$ and $n=18$. Self-interactions in planetary scales $0\leqslant n\leqslant 6$ are rather passive in view of the large kinetic energy content involved except in a few scales ($n\leqslant 11$). Cross-interactions are active in most scales.

1. Introduction

The development of increased computer capability, expanded global data analysis coverage and efficient spectral multiplication techniques (Orszag, 1970; Eliasen *et al.*, 1970) has spurred interest in spectral models for operational weather forecasting and simulation of earth's general circulation (i.e., Machenhauer and Daley, 1972; Bourke, 1974). In these models, meteorological scalar variables are expanded in series with spherical harmonics as basis functions (see Platzman, 1960). There is an urgent requirement for diagnostic studies of real atmosphere energetics processes in the spectral domain so we may better monitor model performance and perhaps be guided in some aspects of the physics to be included in spectral models. There have been several spectral energetics studies where Fourier expansions of data at various latitudes are employed (i.e., Saltzman, 1970; Kanamitsu *et al.*, 1972), but thus far little diagnostic energetics work has been done with expansions of data in spherical harmonics.

Existing data coverage imposes two constraints upon such studies. At present it is not possible to obtain reliable, spatially continuous, global analyses of wind, height, temperature, moisture and surface pressure on a daily basis, although spatially continuous daily analyses of most of these fields can be put together for the Northern Hemisphere (Burrows, 1974). This necessitates assigning conditions of symmetry (even parity) or antisymmetry (odd parity) about the equator to these data fields. Fortunately, this can be done without undue inaccuracy in physical

Unauthenticated | Downloaded 01/19/22 11:11 AM UTC

representation of data fields, except possibly in a small band of latitude about the equator, provided a sufficiently large number of terms are retained in the series expansions. The second constraint also arises from data sparsity. The data spectra become more a function of the analysis procedure than of actual observed data below a certain ill-defined scale limit. For this reason the series expansions must be truncated at reasonably low spectral indices. The truncation limits chosen here are $l=n=24$, where l is the order and n is the degree of the spherical harmonic Y_n^l. This is a "triangular" truncation, chosen so that all l wave components are included for a given value of n, which is an appropriate scale index for representation of atmospheric energy spectra (Baer, 1972; Wiin-Nielsen, 1972). Flow in these scales is quasi-horizontal.

A full and complete analysis of spectral domain energetics processes occurring in our atmosphere is a large project which requires much expenditure of time and money. Only a small sector of the problem will be discussed here, namely, the forces which affect the rates of change with time (tendency) of the individual spectral components of the horizontal total kinetic energy spectrum. As can be seen in the horizontal spectral kinetic energy tendency equations to be derived in Section 2, these forces are the pressure gradient force, the Coriolis force, dissipation and the nonlinear kinetic energy transfer (horizontal advection plus sphericity terms). The latter is of particular interest as it is the mechanism of large-scale turbulent horizontal exchange of kinetic energy among scales of motion. With the spectral representation it is relatively easy to isolate the various scale interactions which give rise to the total nonlinear kinetic energy transfer into or out of a given scale of motion. Results and discussion of this and other calculations are presented in Section 4, which follows a brief discussion of data sources and analysis procedures in Section 3. A summary and conclusions appear in Section 5.

2. Theory

A scalar data field may be expressed in series form as

$$A(\lambda,\mu)=\sum_{l=-L}^{L}\sum_{n=|l|}^{N}A_n^l Y_n^l(\lambda,\mu), \tag{2.1}$$

where λ is longitude, μ is sine of latitude, and

$$Y_n^l(\lambda,\mu)=e^{il\lambda}P_n^l(\mu), \tag{2.2}$$

$$P_n^l(\mu)=\left[\frac{(2n+1)(n-l)!}{(n+l)!}\right]^{\frac{1}{2}}\frac{(1-\mu^2)^{l/2}}{2^n n!}\times\frac{d^{n+l}}{d\mu^{n+l}}(\mu^2-1)^n, \tag{2.3}$$

$$A_n^l=\frac{1}{4\pi}\int_{-1}^{1}\int_{0}^{2\pi}A(\lambda,\mu)Y_n^{l*}(\lambda,\mu)d\lambda d\mu, \tag{2.4}$$

$$Y_n^{l*}(\lambda,\mu)=e^{-il\lambda}P_n^l(\mu). \tag{2.5}$$

The square root factor in (2.3) normalizes the associated Legendre functions $P_n^l(\mu)$ to 2 upon integration over $\mu=-1$ to $+1$. Numerical integration of (2.4) can be performed over an evenly spaced latitude-longitude grid with a Neumann quadrature scheme described by Ellsaesser (1966) for integration over latitude, and the fast Fourier transform for integration over longitude.

Separations of the wind field can be done as follows. The rotational wind components are

$$u_R=-\frac{(1-\mu^2)^{\frac{1}{2}}}{a}\frac{\partial\psi}{\partial\mu}, \tag{2.6}$$

$$v_R=\frac{1}{a(1-\mu^2)^{\frac{1}{2}}}\frac{\partial\psi}{\partial\lambda}, \tag{2.7}$$

where ψ is a streamfunction, a the earth's radius, and u_R and v_R rotational zonal and meridional wind components, respectively. With data given on an evenly spaced latitude-longitude grid, the vorticity field can be calculated at each grid point with a centered finite-difference analogue of the relation

$$\zeta=\frac{1}{a(1-\mu^2)^{\frac{1}{2}}}\frac{\partial v}{\partial\lambda}-\frac{(1-\mu^2)^{\frac{1}{2}}}{a}\frac{\partial u}{\partial\mu}+\frac{\mu u}{a(1-\mu^2)^{\frac{1}{2}}}, \tag{2.8}$$

where ζ is vorticity and u and v are zonal and meridional wind components, respectively. The spectrum of the resulting vorticity field will be accurate to wavenumber $N/4$, where N is the number of longitude grid points (one could increase accuracy to $N/2$ by using Fourier expansions of the wind field derivatives—in this study a 3° resolution data was used, and series were truncated at $l=n=24$ so the method is not crucial). The vorticity field is expanded in a series, and then using the identity

$$\nabla^2 Y_n^l=\frac{-n(n+1)}{a^2}Y_n^l, \tag{2.9}$$

the coefficients of the stream field are

$$\psi_n^l=-\frac{a^2\zeta_n^l}{n(n+1)},\quad n>0,$$
$$=\text{constant}\times n=0. \tag{2.10}$$

The rotational wind spectra are obtained by expanding grid-point values of u_R and v_R which have been calculated from (2.6) and (2.7) with (2.10) and the

Unauthenticated | Downloaded 01/19/22 11:11 AM UTC

identities

$$\frac{\partial Y_n^l}{\partial \lambda}=ilY_n^l, \tag{2.11}$$

$$(1-\mu^2)^{\frac{1}{2}}\frac{\partial Y_n^l}{\partial \mu}=\left\{\frac{(n+1)\mu P_n^l}{(1-\mu^2)^{\frac{1}{2}}}-\left[\frac{(n-l+1)(n+l+1)(2n+1)}{2n+3}\right]^{\frac{1}{2}}\times\frac{P_{n+1}^l}{(1-\mu^2)^{\frac{1}{2}}}\right\}e^{il\lambda}. \tag{2.12}$$

Of course, one cannot obtain grid-point values of u_R and v_R directly at the poles from spectral series because the wind components in this form are not true scalars, but the polar singularities have no effect upon values of the wind elsewhere due to the vanishingly small area involved (see Simmonds, 1974). The divergent wind spectra are obtained by expansion of the grid-point remainder fields

$$u'=u-u_R, \tag{2.13}$$

$$v'=v-v_R. \tag{2.14}$$

The coefficients of the u_D and v_D fields so calculated are valid up to the truncation used for u_R and v_R, as the remainders u' and v' contain those portions of the u_R and v_R spectra described by spectral indices higher than this.

For hemisphere data coverage we must assign parity conditions to scalar data fields. Based on observation, temperature and geopotential height fields are largely symmetric about the equator, and can therefore be assigned even parity. The vertical motion field is best described by an even parity spectral expansion in most months so that details of the Intertropical Convergence Zone (ITCZ), which lies near the equator but generally not on it, are not lost (vertical motion is not considered in this study). Given the even parity of the geopotential height field, the geostrophic wind equations suggest that even parity be assigned to u_R and odd parity to v_R. The divergent wind components can be either parity, although if the vertical motion field is assigned even parity, then we should choose u_D even and v_D odd. In order to best represent the hemispheric data fields it was decided here to expand u' as an odd field and v' as an even field. The resulting spectra are not purely divergent as the odd u' coefficients will contain odd u_R and the even v' coefficients will contain even v_R (one could, however, obtain the even u_D and odd v_D spectral coefficients, but this was not done here). This discrepancy will not significantly alter the results, as the missing wind components are of very small magnitude and no attempt is made here to isolate spectral kinetic energy tendency equations for individual wind components.

The total kinetic energy over a spherical surface is given in terms of the amplitudes of the wind spectra as

$$K=\frac{1}{2}\int_S(u^2+v^2)dS=\tfrac{1}{2}\sum_{l=0}^{L}\sum_{n=l}^{N}(2-\delta_{0l})(u_{R_n}^l u_{R_n}^{-l}+v_{R_n}^l v_{R_n}^{-l}+u_{D_n}^l u_{D_n}^{-l}+v_{D_n}^l v_{D_n}^{-l}), \tag{2.15}$$

where, because wind is a real quantity, $u_{R_n}^{l*}=(-1)^l u_{R_n}^{-l}$, etc. The sum of the cross-products $2u_Ru_D$ and $2v_Rv_D$ vanishes because

$$\int_S \mathbf{k}\times\nabla\psi\cdot\nabla\chi dS=\int_S(\nabla\cdot\mathbf{k}\times\chi\nabla\psi+\chi\nabla\cdot\mathbf{k}\times\nabla\psi)dS=0, \tag{2.16}$$

where χ is a velocity potential, although the individual terms in the cross products do not vanish.

Spectral kinetic energy tendency equations are derived by differentiating (2.15) with respect to time and using the momentum equations in spectral form. Thus

$$\frac{\partial K}{\partial t}=\mathrm{Re}\sum_{l=0}^{L}\sum_{n=l}^{N}(2-\delta_{0l})\left(u_{R_n}^{-l}\frac{\partial u_{R_n}^l}{\partial t}+v_{R_n}^{-l}\frac{\partial v_{R_n}^l}{\partial t}+u_{D_n}^{-l}\frac{\partial u_{D_n}^l}{\partial t}+v_{D_n}^{-l}\frac{\partial v_{D_n}^l}{\partial t}\right), \tag{2.17}$$

where Re denotes the real part of a complex product. The spectral total kinetic energy tendency equations for a given (n,l) spectral component are found from the products

$$\frac{\partial K_{Tnl}}{\partial t}=(2-\delta_{0l})\,\mathrm{Re}\left(u_{R_n}^{-l}\frac{\partial u_{R_n}^l}{\partial t}+u_{D_n}^{-l}\frac{\partial u_{D_n}^l}{\partial t}+v_{R_n}^{-l}\frac{\partial v_{R_n}^l}{\partial t}+v_{D_n}^l\frac{\partial v_{D_n}^l}{\partial t}\right). \tag{2.18}$$

The spectral horizontal momentum equations are derived by substituting series expansions for $u=u_R+u_D$ and $v=v_R+v_D$ into the momentum equations

$$\frac{\partial u}{\partial t}=-\frac{u}{a(1-\mu^2)^{\frac{1}{2}}}\frac{\partial u}{\partial \lambda}-\frac{v}{a}(1-\mu^2)^{\frac{1}{2}}\frac{\partial u}{\partial \mu}+\frac{uv}{a}\frac{\mu}{(1-\mu^2)^{\frac{1}{2}}}+2\Omega\mu v-\frac{g}{a(1-\mu^2)^{\frac{1}{2}}}\frac{\partial Z}{\partial \lambda}+Fu, \tag{2.19}$$

$$\frac{\partial v}{\partial t}=-\frac{u}{a(1-\mu^2)^{\frac{1}{2}}}\frac{\partial v}{\partial \lambda}-\frac{v}{a}(1-\mu^2)^{\frac{1}{2}}\frac{\partial v}{\partial \mu}-\frac{u^2}{a}\frac{\mu}{(1-\mu^2)^{\frac{1}{2}}}-2\Omega\mu u-\frac{g(1-\mu^2)^{\frac{1}{2}}}{a}\frac{\partial Z}{\partial \mu}+Fv, \tag{2.20}$$

and solving for coefficients in the fashion of (2.4). In (2.19) and (2.20) Fu and Fv are dissipation terms, g the acceleration of gravity, Ω the earth's rotation rate and Z height.

Unauthenticated | Downloaded 01/19/22 11:11 AM UTC

Except for dissipation, all terms which arise in the spectral kinetic energy tendency equations can be calculated with a numerical Gaussian quadrature and fast Fourier transform procedure described by Machenhauer and Rasmussen (1972). Dissipation terms will be calculated in this study as a residual between the actual kinetic energy tendency of each spectral component (calculated from data with 24 h centered time differencing) and the sum of all other terms in each respective tendency equation. The meaning of dissipation, when calculated as a residual, will be uncertain because other terms are "instantaneous." However, the dissipation residuals should be partially representative of the influence of scales smaller than $n=24$ upon the respective energy tendencies.

A process of considerable interest in the spectral kinetic energy tendency equations is the nonlinear horizontal transfer of kinetic energy (sum of horizontal advection and sphericity terms), as this is the process of large-scale turbulent transfer of kinetic energy among scales of motion. The total transfer of kinetic energy into or out of a scale of motion by the nonlinear transfer terms is the sum of transfers by interactions of motion in all scales. By isolating some of these interactions we can assess the importance of the scales involved to the maintenance of kinetic energy in all scales. This information can be particularly useful for assessing the impact of truncation and subgrid-scale diffusion parameterization in spectral models of the atmosphere. The scale range $0\leqslant n\leqslant 24$ may be divided (somewhat arbitrarily) into planetary ($0\leqslant n\leqslant 6$), synoptic ($7\leqslant n\leqslant 14$) and small-synoptic ($15\leqslant n\leqslant 24$) scale ranges based on Baer's (1972) calculations of growth rates of the kinetic energy of wave perturbations superimposed individually upon a zonally vertically averaged basic flow using the linearized potential vorticity equation at five levels in the atmosphere. (Each scale index n includes all coefficients with $l\leqslant n$ in series summations.) Restrictions of summation over n to the three aforementioned scale ranges in nonlinear terms results in six independent types of interactions which give rise to the total nonlinear kinetic energy transfer seen in each scale. Three of these are "self-interactions" (interaction of motion in the same scale range), and three of these are "cross-interactions" (interaction of motion in different scale ranges).

An interesting feature of the equations is that the Coriolis terms do not vanish in each n scale but only when the equations are summed over all n up to the truncation limit. This can be seen from the identity

$$\mu P_n^l=\left[\frac{(n-l+1)(n+l+1)}{(2n+1)(2n+3)}\right]^{\frac{1}{2}}P_{n+1}^l+\left[\frac{(n+l)(n+l)}{(2n+1)(2n-1)}\right]^{\frac{1}{2}}P_{n-1}^l \quad (2.23)$$

which arises in Coriolis terms. Contributions to Coriolis terms in a given scale n come from adjacent scales $n-1$ and $n+1$.

With the assumption of even parity for the Z field and neglect of even u_D and odd v_D we cannot calculate the generation of kinetic energy from available potential energy by the pressure gradient term $-g\mathbf{V}_D\cdot\nabla Z$. The pressure gradient term that does appear is $-g\mathbf{V}_R\cdot\nabla Z$, which vanishes upon integration over a sphere. It represents the process of adjustment of the mass and rotational wind fields which have been thrown out of balance by processes that generate and consume available potential energy and by turbulent transfers of kinetic energy among scales of motion, all of which occur on different time scales.

3. Data

Due to computer time limitations, only two weeks of data were used for the summer period—00 GMT 1 August to 12 GMT 15 August 1970, at the surface, 850, 700, 500, 300, 250, 200 and 100 mb. Wind analyses by National Meteorological Center (NMC) were obtained from National Center for Atmospheric Research[1] (NCAR) for the NMC octagonal grid (Shuman and Hovermale, 1968) and tropical 5° resolution grid (Bedient *et al.*, 1967). Height analyses were obtained from the U. S. Navy Fleet Numerical Weather Center (FNWC) for their Northern Hemisphere grid. All analyses were interpolated by 16-point Bessel interpolation to a 3° resolution grid. The NMC analyses were merged with a linear weighting scheme in the zone 27°–33°N, as this latitude belt gave a somewhat more accurate hemispheric wind analysis than more southerly merging zones (Burrows, 1974). August climatology was used at the surface and in the tropics at 850 and 100 mb. Due to missing data, calculations could not be done for August 1/12 GMT, 5/10 GMT, 5/12 GMT, 7/00 GMT and 13/00 GMT. At five other times either a u or v NMC tropical wind analysis was missing at a single pressure level. Data were filled in with the average of the missing fields 12 h before and 12 h after the missing times.

4. Results and discussion

When interpreting results, we should bear in mind the following conditions. First, only two weeks of data were used so the results should be regarded only as an indication of summer spectral kinetic energetics. Second, due to the parity assumptions necessary because of a lack of Southern Hemisphere data, the results may differ slightly from results based on a global data set. Third, data accuracy could be questioned in the smallest scales ($n>18$) because of the 5° resolution of tropical data. Fourth, results are

[1] National Center for Atmospheric Science is sponsored by National Science Foundation.

Unauthenticated | Downloaded 01/19/22 11:11 AM UTC

scaled by the n index by summation over all $l \leqslant n$ components for each n, and may not resemble existing calculations where scaling by l index was employed (i.e., Saltzman, 1970; Kanamitsu *et al.*, 1972). The n index is two-dimensional and embodies two one-dimensional indices, l (number of zeros of Y_n^l around a latitude circle) and $n-l$ (number of zeros of Y_n^l between the poles).

a. Kinetic energy spectra

Time-vertically averaged kinetic energy spectra are shown in Table 1. Numbers in column 2 are total kinetic energy (K_{T_n}) in each scale n (summed over all $l \leqslant n$ components), numbers in other columns are percent of K_{T_n}. It should be recalled that the u_{D_n} and v_{D_n} wind components in Table 1 are not wholly divergent, although they are of the same order of magnitude as divergent wind components would be.

Maxima of K_{T_n} occur at $n=2$ and 4 with a smaller maximum at $n=9$. Relatively little kinetic energy resides in the planetary average flow ($n=0$) because a large belt of tropical easterlies in summer largely cancels the mid-latitude westerlies in the global average. Baer (1972) found kinetic energy maxima at $n=0$, 4 and 10 for winter data. In his results and those in Table 1 there is a rapid fluctuation of kinetic energy in adjacent even and odd scales for $n<8$. Some of this may be due to the assumption of even parity for u_R (although u_R is largely an even field, even if global observations had been used). u_R contains most of the kinetic energy in each scale up to $n=7$, the scale where equipartition of u and v kinetic energy occurs. Charney (1971) predicted equipartition of u and v scale kinetic energy in scales sufficiently far removed from the basic flow in quasi-geostrophic flow. Most of the scale kinetic energy resides in the rotational wind components up to $n=23$, 24.

Time-averaged kinetic energy spectra at each pressure level are not shown to save space. Most kinetic energy is contained in the scales $n=2$ and 4 from 700 to 100 mb, with $n=2$ much more dominant (33%) at 100 mb. At 850 mb, where baroclinicity and boundary layer effects are strong, $n=6$ contains more kinetic energy than other scales and there is a more proportionate distribution of kinetic energy among all scales $n \leqslant 6$ than at other pressure levels. For the surface climatological data, $n=2$ and $n=3$ contain more kinetic energy than other scales, possibly due to the influence of continents. Equipartition of u and v kinetic energy extends to $n=0$ at the surface, but occurs elsewhere around $n=7$.

The slope of kinetic energy with n was calculated for the small synoptic scales $15 \leqslant n \leqslant 24$ by fitting the data with a power law of the form

$$K_n = An^b, \tag{4.1}$$

where K_n is the kinetic energy of a wind component

TABLE 1. Time-average kinetic energy in each scale of motion (K_{T_n}: units m^2 s^{-2}), percent in each scale of total kinetic energy summed over all n up to $n=24$, and percent of K_{T_n} in wind components vertically averaged from surface to 100 mb.

n	K_{T_n}	Percent of total kinetic energy	Percent of K_{T_n} in each of the components					
			$K(u_{R_n})$	$K(u_{D_n})$	$K(v_{R_n})$	$K(v_{D_n})$	$K(u_n)$	$K(v_n)$
0	1.720	2.98	99.17	0.00	00.00	0.83	99.17	0.85
1	0.3349	0.58	73.53	0.21	0.00	26.25	73.75	26.25
2	10.56	18.26	94.55	1.96	2.92	0.57	96.52	3.48
3	1.770	3.06	67.73	6.74	19.49	6.03	74.47	25.53
4	6.838	11.82	93.48	0.91	4.31	1.31	94.39	5.61
5	1.122	1.94	63.12	5.03	26.30	5.55	68.15	31.85
6	2.696	4.66	76.73	2.66	17.82	2.79	79.40	20.60
7	1.545	2.67	54.14	3.58	37.58	4.69	57.73	42.27
8	3.227	5.58	55.51	1.79	40.72	1.97	57.30	42.70
9	3.463	5.99	57.46	1.76	39.08	1.70	59.22	40.78
10	3.008	5.20	34.56	2.16	61.30	1.98	36.72	63.28
11	2.897	4.98	50.22	1.93	45.99	1.86	52.14	47.86
12	2.648	4.58	48.31	2.10	47.51	2.07	50.42	49.58
13	2.312	4.00	56.01	2.59	39.11	2.28	58.60	41.40
14	2.163	3.74	50.73	3.10	43.89	2.29	53.82	46.18
15	1.787	3.09	52.07	3.48	41.82	2.63	55.55	44.45
16	1.760	3.04	43.30	3.45	50.67	2.58	46.75	53.25
17	1.461	2.53	48.83	3.79	44.14	3.25	52.61	47.39
18	1.409	2.44	47.44	4.15	45.41	2.99	51.60	48.40
19	1.182	2.04	48.51	4.78	43.34	3.37	53.29	46.71
20	1.019	1.76	49.06	5.29	41.48	4.17	54.34	45.66
21	0.8343	1.44	43.80	6.44	44.91	4.85	50.24	49.76
22	0.6796	1.18	37.86	7.11	49.35	5.67	44.97	55.03
23	0.7116	1.23	31.67	26.13	37.02	5.18	57.80	42.20
24	0.6983	1.21	27.73	20.22	32.84	19.21	47.95	52.05

Unauthenticated | Downloaded 01/19/22 11:11 AM UTC

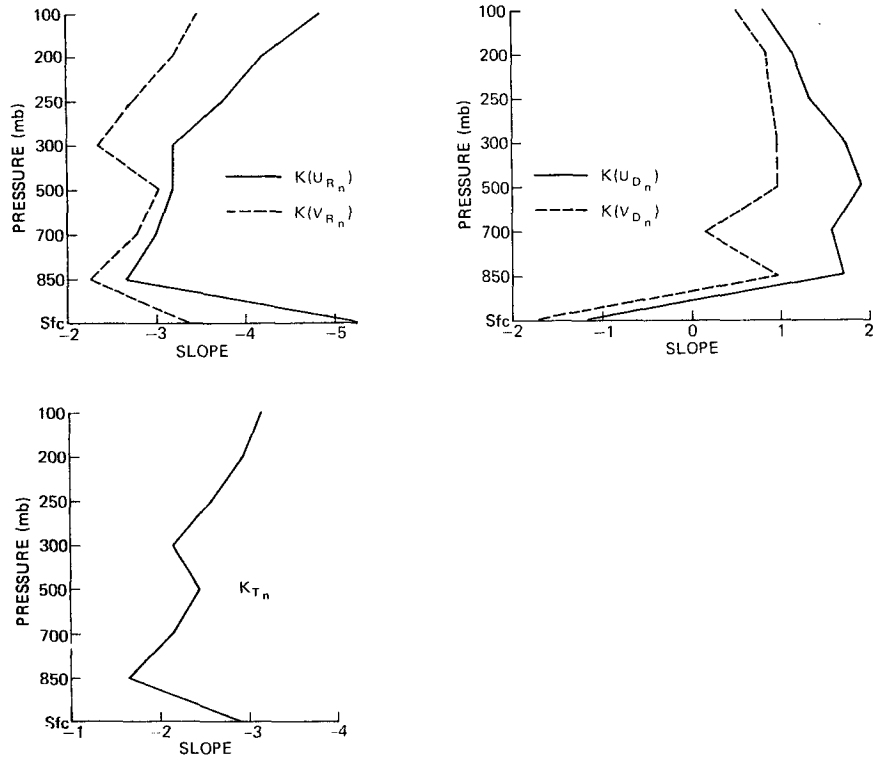

FIG. 1. Time-average slopes of the kinetic energy of wind components with scale n in scales $15 \leqslant n \leqslant 24$.

in scale n, and A and b are constants. Results are shown in Fig. 1.

The slope of $K(u_{R_n})$ is close to -3 from 700 to 300 mb, while the slope of $K(v_{R_n})$ is close to -3 at 700, 500 and 200 mb. The slope of total kinetic energy K_{T_n} is close to -3 only at 200 mb. The slopes of $K(u_{D_n})$ and $K(v_{D_n})$ are positive except for the surface climatological data. There is a dramatic increase in the slopes of rotational wind components at the tropopause. Insofar as data accuracy is accepted, it appears that motion in these scales cannot be explained by two-dimensional isotropic turbulence theory (which predicts a -3 slope for the rotational wind) except around the tropopause level.

b. Kinetic energy tendencies

Tendencies at 850, 500 and 200 mb are shown in Tables 2, 3 and 4, respectively. Summed tendencies in column 2 are the order 10^{-5} m^2 s^{-3} in the lower troposphere (10^{-6} m^2 s^{-3} in smaller and very large scales), 10^{-5} m^2 s^{-3} in the middle troposphere (10^{-4} m^2 s^{-3} in some synoptic scales), and 10^{-4} m^2 s^{-3} in the upper troposphere (10^{-5} m^2 s^{-3} in smaller and very large scales). The relative importance of the terms in the equation can largely be anticipated by scale analysis in each scale of motion. The dissipation remainder is equal and opposite to the sum of all other terms, indicating the importance of fluxes of kinetic energy between scales $n \leqslant 24$ and subgrid scales $n > 24$. Of the remaining terms, the pressure gradient and Coriolis terms are largest overall, with zonal and meridional advection generally second to these, except in very large scales $n < 3$. In Table 4, the scale $n = 2$, which contains 18.7% of all kinetic energy in the scales $n \leqslant 24$ at 200 mb, appears to be forced by nonlinear transfer of kinetic energy by meridional advection from other scales of motion with the pressure gradient force acting to remove the excess kinetic energy. The terms are rarely of the same sign, suggesting that kinetic energy in each scale of motion is maintained by a complex interplay of physical processes.

To illustrate the active spectral ranges (large-summed kinetic energy tendency) in Tables 2, 3 and 4 (and for other portions of the atmosphere where results are not shown), the tendencies at each pressure level are shown in Fig. 2 as a percentage of the largest tendency in the range $0 \leqslant n \leqslant 24$ at each pressure level. Single bars denote values $\geqslant |25\%|$, double bars denote values $\geqslant |50\%|$ and positive tendency areas are shaded. Some of the active scales are separated by only 1 or 2 scales indices—this may be due to parity assumptions, particularly for $n \leqslant 7$. There is a fairly continuous spectrum of active scales in the range $3 \leqslant n \leqslant 18$ in the lower and middle troposphere. Activity in the smaller scales $n \geqslant 12$ gradually dies out above 500 mb and becomes more selective ($n = 0$, 3–6 and 10–12). These results are in fairly good agreement with theoretical studies of the atmosphere. Kuo (1953)

Unauthenticated | Downloaded 01/19/22 11:11 AM UTC

TABLE 2. Time-average tendencies for K_{T_n} at 850 mb. Tendencies in column 2 are the sum of all terms except the "dissipation residual" terms (DIS), with l dependence summed out for each n. Numbers in columns 3 to 8 are percentages of the number in column 2. ZA stands for zonal advection, MA for meridional advection, SPH for sphericity, COR for Coriolis and PG for pressure gradient. Units in columns 2 are 10^{-8} m^2 s^{-3}, units in columns 3 to 8 are percent. Due to roundoff error, the sum of the percentages in columns 3 to 7 may be slightly different from 100%.

		K_{T_n} tendency equation terms at 850 mb					
n	$\frac{\partial K_{T_n}}{\partial t}$	ZA	MA	SPH	COR	PG	DIS
0	1	1338.0	−1276.6	−134 2	172.5	0.0	−1055.7
1	903	0.9	0.2	0.2	51 3	41.8	−93.4
2	781	−0.4	−50.1	0.1	−16.4	166.9	−85.6
3	−653	−6.8	−13.5	3.3	236.1	−119.1	−104.6
4	61	176.1	99.2	44.7	−226.9	6.9	−28.5
5	784	−3.3	27.8	1.4	−1.4	75.5	−97.2
6	4080	1.5	−12.4	−0.0	32.9	78.0	−102.6
7	−1900	−0.3	0.0	0.9	−16.9	116.3	−102.6
8	1195	1.5	12.7	−1.3	−13.1	100.3	−83.3
9	−2303	−4.1	6.9	−0.6	0.4	97.3	−102.5
10	−1968	2.6	1.3	1.0	−31.7	126.5	−105.6
11	−2144	10.7	−2.7	0.3	4.2	87.5	−104.4
12	−1351	−3.5	9.1	−0.2	38.9	55.7	−98.0
13	867	−0.1	−13.6	−1.1	−25.0	139.8	−99.0
14	−3676	2.9	2.9	−0.1	19.4	74.9	−102.0
15	1927	0.9	−0.6	0.6	6.2	92.9	−100.9
16	1208	−3.2	−6.8	0.5	86.8	22.8	−97.0
17	−1046	−2.9	−12.0	−0.7	−22.5	138.0	−104.0
18	−1761	−3.9	2.7	−0.2	12.1	89.2	−102.0
19	39	−219.8	−329.9	9.5	−889.9	1530.1	−176.4
20	261	7.2	9.2	−1.0	−36.7	120.7	−113.2
21	−855	4.2	7.7	−0.7	28.2	60.5	−99.1
22	107	24.2	−118.2	−4.8	280.5	−81.6	−102.3
23	−294	−0.1	14.3	−0.0	12.0	73.8	−110.2
24	134	9.7	−55.7	3.3	−3.4	146.0	−84.0

TABLE 3. As in Table 2 except for K_{T_n} tendencies at 500 mb.

		K_{T_n} tendency equation terms at 500 mb					
n	$\frac{\partial K_{T_n}}{\partial t}$	ZA	MA	SPH	COR	PG	DIS
0	559	0.7	96.2	1.1	2.0	0	−77.2
1	492	6.4	−19.6	0.9	13.5	98.7	−97.0
2	938	3.7	−58.8	5.8	62.9	86.4	−98.3
3	−2023	0.5	−0.6	2.1	16.0	82.0	−100.2
4	4368	0.8	−4.4	0.4	29.6	73.6	−104.8
5	−1156	8.3	1.1	3.3	67.7	19.7	−98.2
6	−1570	10.2	22.0	−3.7	−75.6	147.1	−104.7
7	431	102.7	−1.3	11.6	−564.5	551.5	−72.6
8	6585	4.2	4.6	−0.4	16.4	75.1	−97.9
9	634	−0.9	2.1	−14.2	365.5	−252.5	−97.8
10	−2080	−8.3	−18.1	1.0	−49.0	174.5	−97.6
11	−6372	0.3	−7.0	0.1	57.5	48.5	−100.8
12	4419	8.3	−2.5	−0.7	−8.6	103.5	−99.5
13	−5612	6.1	−2.8	−0.2	63.7	27.6	−99.1
14	−2334	22.7	−43.6	−0.1	−29.5	150.6	−100.7
15	4782	−2.3	−6.4	2.0	−5.3	112.0	−100.2
16	2800	−1.0	11.1	−1.0	97.8	−6.9	−101.6
17	−1109	−1.5	−78.3	2.1	−34.6	212.3	−103.5
18	−292	−5.2	46.3	7.0	−294.2	346.0	−77.3
19	1475	−3.4	2.1	0.1	−6.9	108.2	−96.8
20	830	−3.4	−1.6	2.5	−56.5	159.0	−99.3
21	−1938	−6.7	−11.9	0.2	36.8	81.6	−101.8
22	1314	2.5	6.0	0.7	49.9	41.0	−97.1
23	43	−7.8	191.4	−1.8	178.9	−260.7	−77.0
24	−1169	−4.2	8.9	0.2	21.8	73.4	−101.8

Unauthenticated | Downloaded 01/19/22 11:11 AM UTC

TABLE 4. As in Table 2 except for K_{T_n} tendencies at 200 mb.

n	$\frac{\partial K_{T_n}}{\partial t}$	K_{T_n} tendency equation terms at 200 mb ZA	MA	SPH	COR	PG	DIS
0	10 057	−0.2	100.0	−0.9	1.2	0	−95.4
1	1304	44.2	52.1	−6.2	−41.2	51.1	−95.1
2	−782	18.7	−1509.8	−17.9	276.2	1332.7	−147.6
3	17 403	−2.9	17.2	1.6	−7.7	91.7	−99.9
4	−13 128	−2.3	11.8	0.4	86.8	3.4	−96.8
5	−3 243	−44.5	137.8	−22.5	−177.3	206.4	−109.2
6	−12 208	0.6	19.1	−0.6	−7.3	88.3	−101.7
7	7228	−12.4	−33.0	−4.2	73.8	73.7	−102.7
8	3835	19.5	−94.9	1.2	−100.1	274.4	−93.9
9	−6019	−10.7	78.1	18.6	−78.6	92.6	−96.1
10	15 999	−13.5	0.6	−6.5	26.5	93.0	−98.0
11	−35 027	−5.3	6.8	−0.4	5.3	93.5	−99.7
12	17 761	9.3	3.3	−0.2	15.3	72.3	−100.5
13	−10 280	16.7	−1.9	−7.5	38.5	54.2	−96.9
14	−3280	64 4	13.9	−0.3	10.1	11.8	−106.3
15	−5709	17.4	15.8	−2.7	1.1	68.3	−94.9
16	2574	−2.6	22.0	−1.3	172.6	−90.7	−99.2
17	6387	1.4	21.8	−1.3	−0.4	78.5	−100.1
18	−2488	27.7	32.6	1.4	−113.2	151.4	−98.8
19	−995	8.1	−105.4	1.4	141.1	54.8	−113.5
20	4131	14.6	8.5	0.4	−13.8	90.4	−101.3
21	−4059	−0.7	−26.3	0.7	63.0	63.2	−100.5
22	−1909	4.4	−8.4	−4.1	58.8	49.2	−99.7
23	−2143	−7.4	21.6	−1.8	−14.8	102.3	−101.9
24	−1093	−75.4	19.8	−0.8	4.9	151.5	−110.2

found disturbances with wavelengths 2000–4000 km are unstable below 700 mb in a baroclinic atmosphere, but instability dies out above 700 mb in the shorter scales in favor of disturbances with wavelengths $\geqslant$7200 km in the upper troposphere. Brown (1969a, b) found similar results for a baroclinic-barotropic atmosphere. In addition he found two distinct spectral regions of maximum instability, which may account for the selectivity of active scales seen here in the middle and upper troposphere.

The vertically integrated nonlinear horizontal transfers of kinetic energy (sum of advection and sphericity terms in the tendency equations) calculated here for the n domain are shown in Table 5 along with Saltz-

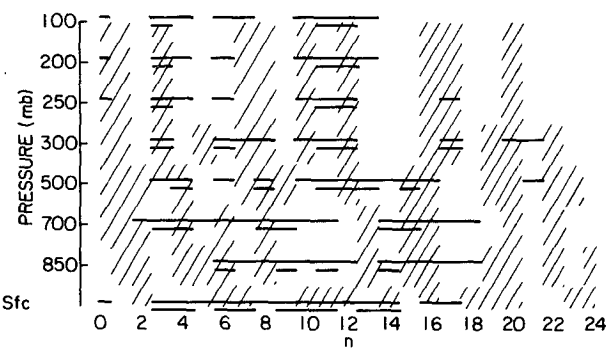

FIG. 2. Scales at each pressure level where relatively large tendencies occur. Single bars denote values $\geqslant|25\%|$ of large tendency at a pressure level, double bars values $\geqslant|50\%|$. Positive areas are shaded.

TABLE 5. Total kinetic energy tendencies in Northern Hemisphere summer due to horizontal nonlinear transfer of kinetic energy. Saltzman (1970) is for l domain in extratropical latitudes, Kanamitsu *et al.* (1972) is for l domain in the tropics, Burrows is in n domain (two-dimensional). Saltzman and Burrows are vertically integrated, with units ergs cm^{-2} s^{-1}. Kanamitsu *et al.* is at 200 mb, units 10^{-5} m^2 s^{-3}.

Scale	Saltzman	Kanamitsu *et al.*	Burrows
0	650	0.18	304
1	−10	−3.32	35
2	−120	−0.12	130
3	−10	0.50	90
4	−70	0.63	−39
5	−30	0.88	−56
6	−160	1.03	−80
7	−120	0.53	−113
8	−100	0.78	−52
9	−60	0.62	−122
10	−60	0.58	−90
11	−20	0.41	9
12	10	0.33	60
13	40	0.11	−57
14	40	0.17	−76
15	50	0.25	−86
16			21
17			66
18			−82
19			31
20			29
21			54
22			1
23			−13
24			18

Unauthenticated | Downloaded 01/19/22 11:11 AM UTC

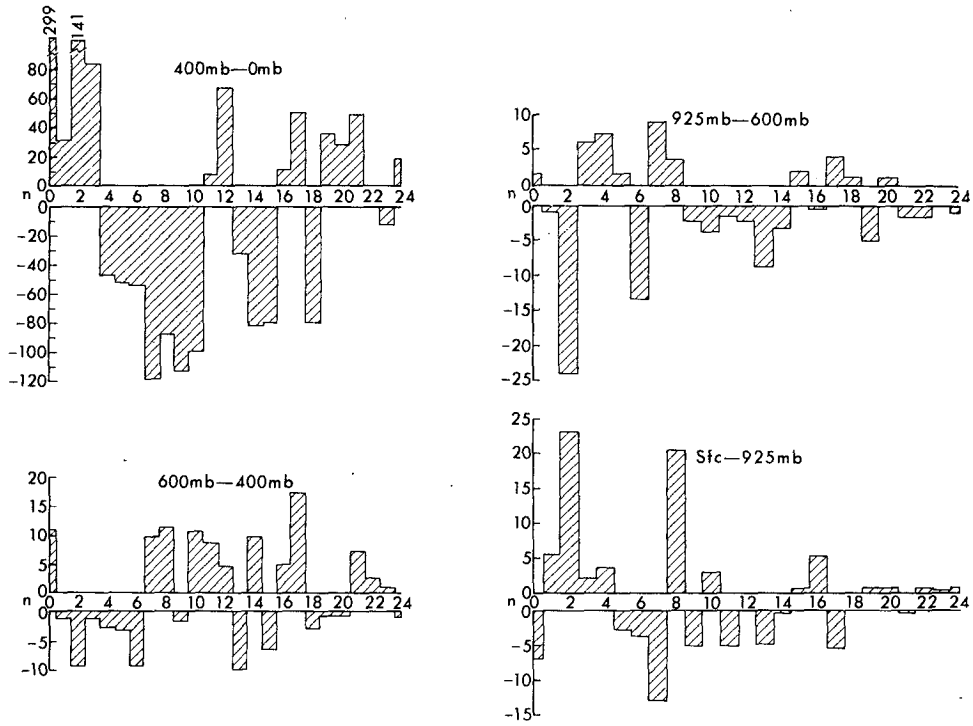

FIG. 3. Pressure-integrated nonlinear horizontal transfer of kinetic energy in each scale (n) in layers. Units for ordinate are ergs cm^{-2} s^{-1}. Note the different ordinal scales for the layers.

man's (1970) summary of vertically integrated l domain transfers for extratropical latitudes in the Northern Hemisphere summer and those of Kanamitsu *et al.* (1972) for the tropics at 200 mb in summer (not vertically integrated). The tropical transfers at 200 mb should be representative of the vertically integrated transfer, as the contribution by the upper troposphere overwhelms contributions from other portions of the atmosphere. In the tropics, kinetic energy is generated in the largest scales $l=0$, 1, 2 and transferred to smaller scales, whereas in extratropical latitudes kinetic energy is generated in scales $1\leqslant l\leqslant 11$ and transferred mainly to the zonal ($l=0$) flow and, to a lesser extent, to smaller scales $l>11$. The n domain transfer is more complicated since it consists of kinetic transfers in both regions and additional scales $16\leqslant n\leqslant 24$ were included. There are two kinetic energy source bands ($4\leqslant n\leqslant 10$ and $13\leqslant n\leqslant 15$), a strong source at $n=18$ and a weak source at $n=23$ (data accuracy may be questioned here). The presence of the latter sources suggests the spectral region $n>14$ is not an "inertial subrange."

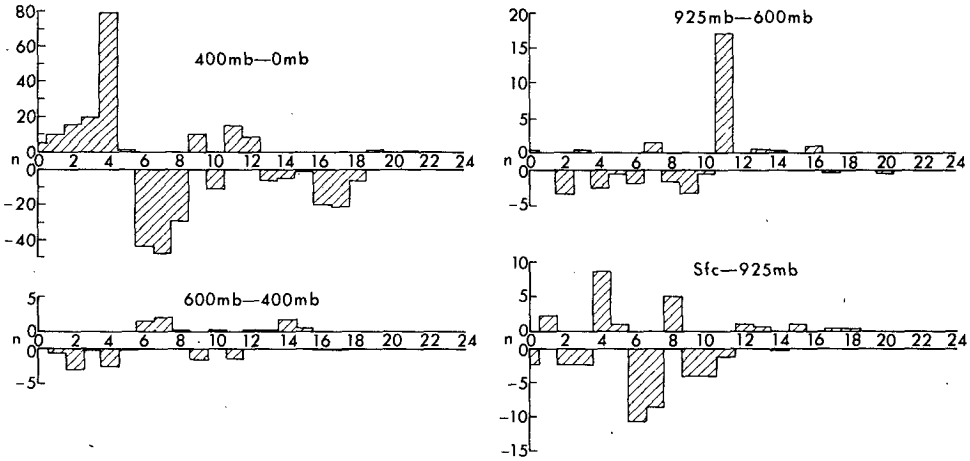

FIG. 4. As in Fig. 3 except for horizontal transfer of kinetic energy by self-interaction (0–6)(0–6) in layers.

Unauthenticated | Downloaded 01/19/22 11:11 AM UTC

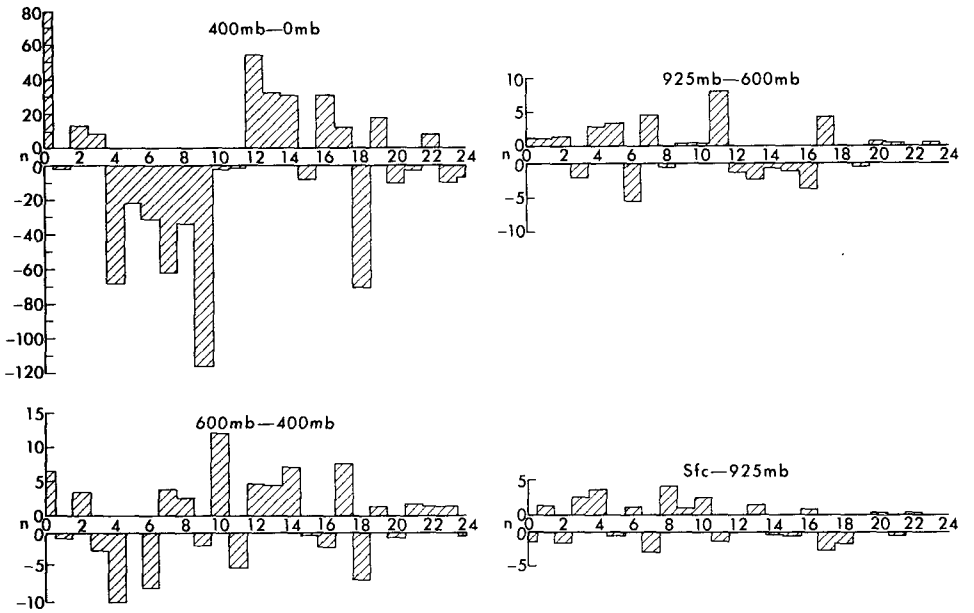

FIG. 5. As in Fig. 3 except for horizontal transfer of kinetic energy by self-interaction (7–14)(7–14) in layers.

The strong source at $n=18$ may be due to the ITCZ, which affects a latitude belt of about 10° (one-tenth of the distance between the poles) and circumscribes the tropics, so that its one dimensional indices are $n-l\approx 18$ and $l\approx 0$, thus $n\approx 18$. The maximum kinetic energy losses in the n domain occur in scales $n=7$ and 9. These peaks are compatible with losses in somewhat lower index scales in the l domain in extratropical latitudes, as the earth's circumference is less in those latitudes than is the global circumference.

In Table 5 the largest scales $0\leqslant n\leqslant 3$ gain kinetic energy from the smaller scales, whereas a transfer to the zonal flow occurs only in extratropical latitudes in the l domain. We recall from Table 1 that $n=2$ contains more kinetic energy than any other scale, whereas in the l domain, the zonal flow contains the most kinetic energy (Saltzman and Fleisher, 1962). The total gain of kinetic energy by the scales $0\leqslant n\leqslant 3$ is 559 ergs cm^{-2} s^{-1} by nonlinear horizontal transfer, which is less than the gain in extratropical latitudes by the zonal flow, because $l=0$ weakly loses kinetic energy in the tropics. From these results it appears that the flow in scales $0\leqslant n\leqslant 3$ behaves like the zonal flow in l domain calculations, as the latitudinal dependence of the latter is lost by averaging over several latitude circles.

Fig. 3 shows a separation of the contributions by lower, middle and upper troposphere to the vertically

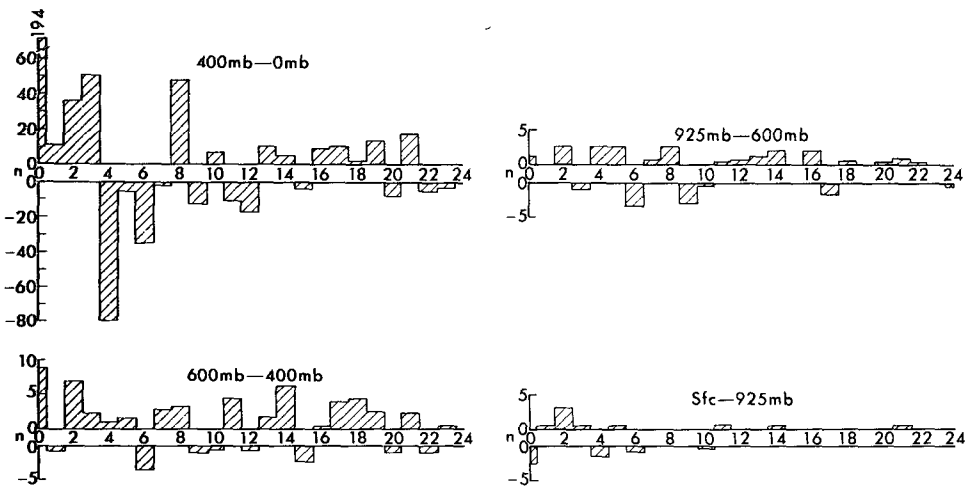

FIG. 6. As in Fig. 3 except for horizontal transfer of kinetic energy by self-interaction (15–24)(15–24) in layers.

Unauthenticated | Downloaded 01/19/22 11:11 AM UTC

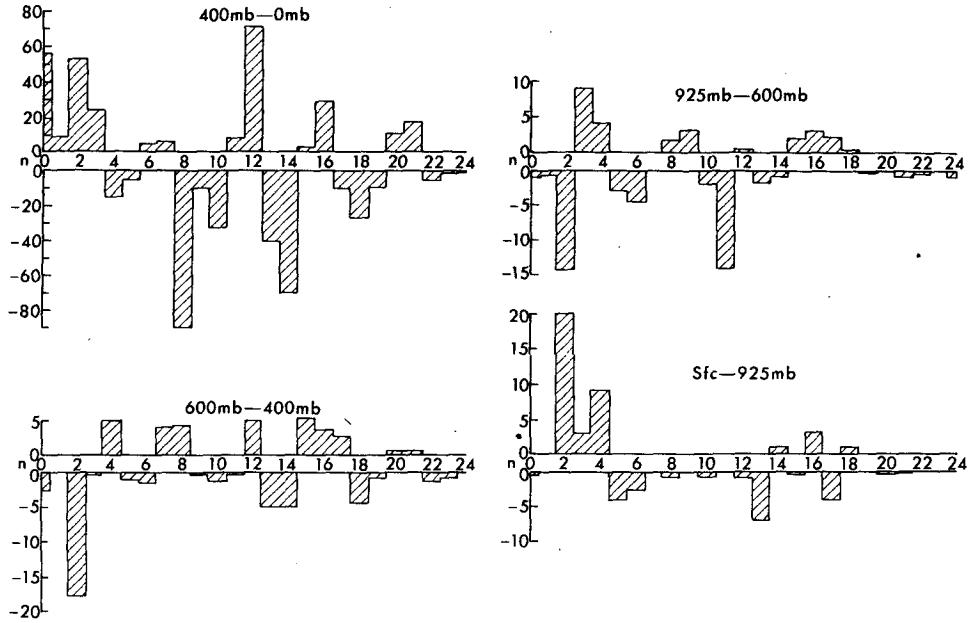

FIG. 7. As in Fig. 3 except for horizontal transfer of kinetic energy by cross-interaction (0–6)(7–14) in layers.

integrated horizontal kinetic energy transfers. By far the greatest contribution comes from the upper troposphere (400–0 mb), due to the higher wind speeds there. There is a considerable difference in the spectral indices of sources and sinks of kinetic energy from the surface to the upper troposphere. A notable feature is a strong loss of kinetic energy by $n=2$ from 925 to 600 mb which is completely masked in the vertical average. In Table 5 a strong loss of kinetic energy by $l=2$ occurs in extratropical latitudes and $l=1$ in tropical latitudes. Saltzman (1970) and Kanamitsu *et al.* (1972) attribute this to land-sea contrasts. The surface climatological data shows a large gain by $n=2$ that could be due to forcing of the flow by continents, which act as barriers to the planetary average ($n=0$) flow, and to transfer from scales smaller than $n=4$.

The scales $0\leqslant n\leqslant 24$ were separated into three ranges: $0\leqslant n\leqslant 6$ (planetary), $7\leqslant n\leqslant 14$ (synoptic) and $15\leqslant n\leqslant 24$ (small-synoptic). By restricting n summation to these ranges in nonlinear terms there result six classes of interactions which give rise to the total nonlinear horizontal transfers of kinetic energy seen in Table 5. These are self-interactions (0–6)(0–6), (7–14)(7–14), (15–24)(15–24) and cross-interactions (0–6)(7–14), (0–6)(15–24), (7–14)(15–24), where, for example, (0–6) stands for

$$\sum_{n=0}^{6}\sum_{l=-n}^{n}.$$

The permutation of each cross-interaction is added to that cross-interaction [i.e., (7–14)(0–6) is added to (0–6)(7–14), because the same two scale ranges are interacting]. Results are shown in Figs. 4–9. There is

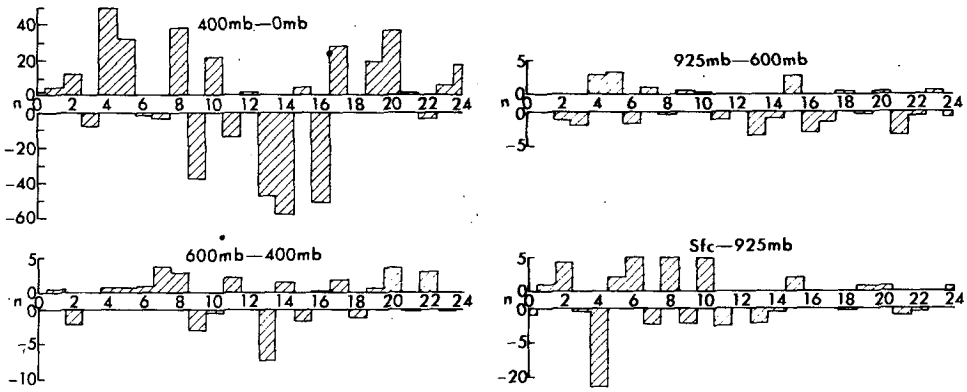

FIG. 8. As in Fig. 3 except for horizontal transfer of kinetic energy by cross-interaction (0–6)(15–24) in layers.

Unauthenticated | Downloaded 01/19/22 11:11 AM UTC

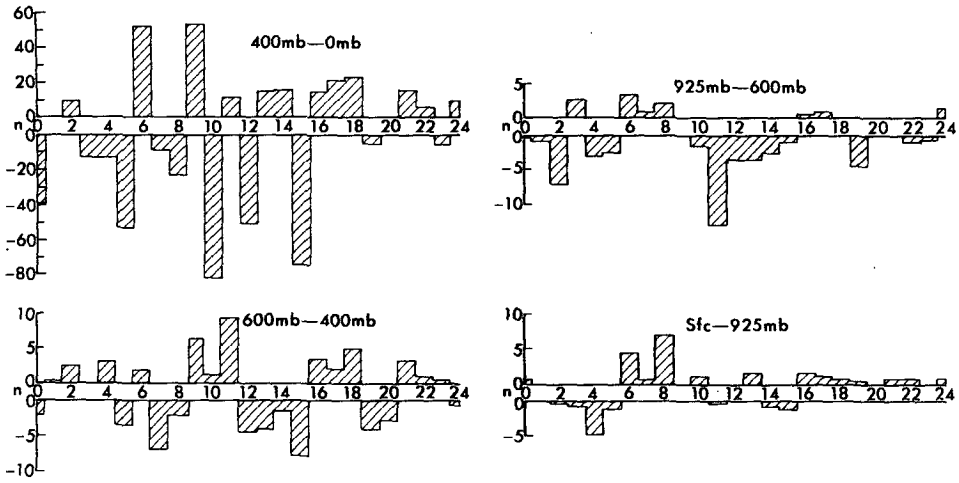

FIG. 9. As in Fig. 3 except for horizontal transfer of kinetic energy by cross-interaction (7–14)(15–24) in layers.

a complex array of kinetic and energy transfers occurring by the various interactions, and very few instances where contributions of all six interaction types are of the same sign in a layer. While it is possible to go into much detail, only the gross features seen in Figs. 4 to 9 will be noted here. These are as follows:

1) Interactions involving the small-synoptic scales $15 \leqslant n \leqslant 24$ are surprisingly active in view of the relatively small kinetic energy content in these scales. The (15–24)(15–24) self-interaction transfers a great deal of kinetic energy to very large scales $n \leqslant 3$ and out of $n=4$ in the upper troposphere. It is responsible for two-thirds of the kinetic energy gain by the planetary average flow ($n=0$) in the upper troposphere. It has been observed in general circulation experiments that increased horizontal grid resolution has a pronounced effect upon ultra-long scales of motion (Miyakoda *et al.*, 1971; Wellck *et al.*, 1971). A partial explanation of this may be that a significant amount of kinetic energy is transferred into ultra-long scales by "self-interaction" of motion in the smaller scales included in the finer resolution experiments. There is also the implication that dissipation parameterizations incorporated into smaller scales of motion in general circulation models will profoundly affect the simulation by the models of large-scale flow features seen in the real atmosphere.

2) Interactions involving scales $7 \leqslant n \leqslant 14$ (scale of baroclinically unstable extratropical disturbances) are generally active. The (7–14)(7–14) self-interaction is quite important and accounts for much of the transfer of kinetic energy out of the scales $4 \leqslant n \leqslant 9$ and $n=18$.

3) All cross-interactions are active in many scales $0 \leqslant n \leqslant 24$, as would be expected from the concept of turbulent supersition of motion in different scales.

4) The self-interaction of planetary scales $0 \leqslant n \leqslant 6$ is rather passive (in view of the large kinetic energy content of these scales) except in scales $n=4$, 6, 7, 8 in the upper troposphere and $n=11$ in the lower troposphere.

5) Much of the activity in $n=2$ (scale of continental land-sea circulation) from the surface to 400 mb occurs by the cross-interaction (0–6)(7–14) of planetary and synoptic scales.

5. Summary and conclusions

Wind spectra are obtained from analyses of observed data, using spherical harmonics expansions. Equations governing the tendencies of kinetic energy of the spectral components of the wind are derived, and a procedure is described for calculation of interactions of various scales of motion in nonlinear terms. Calculations are greatly simplified by use of the transform procedure described by Machenhauer and Rasmussen (1972) and Orszag (1970). Dissipation is obtained as a residual. Results are scaled by the two-dimensional scaling index n (degree of associated Legendre function (P_n^l)).

Calculations were performed with two weeks of data pre-analyzed at grid points for 1–15 August 1970, at eight pressure levels from surface to 100 mb. The data are for the Northern Hemisphere, thus parity assumptions are necessary for scalar data fields and were assigned from the geostrophic wind relationship and observation. A triangular truncation $l=n=24$ of spectral expansions was employed, as data spectra are more a function of analysis procedure than of real data for scales smaller than this. Data accuracy in the higher spectral components considered here may be questionable as the scale limit of data reliability is rather ill-defined.

Due to the short sampling time, results should be regarded as indicative of summer spectral kinetic ener-

Unauthenticated | Downloaded 01/19/22 11:11 AM UTC

getics. Also, as the scaling index n is two-dimensional, results shown here are a combination of the kinetic energetics of tropical and extratropical circulations.

Above 850 mb, maximum kinetic energy resides in the scales $n=2$ and 4, with a secondary maximum at $n=9$. Equipartition of u and v kinetic energy occurs at $n=7$ everywhere but the surface, where climatology was used. Slopes of total kinetic energy with scale for $15\leqslant n\leqslant 24$ are less than -3 everywhere but at 100 mb, and are close to -3 only at 200 mb and the surface.

Total kinetic energy tendencies are generally dominated by the Coriolis and pressure gradient terms, with horizontal nonlinear transfer second, except in scales $n\leqslant 3$. (The Coriolis term does not vanish in individual n scales, but does vanish when summed over all n up to the truncation limits.) The dissipation residuals are always nearly opposite and equal to the sum of the other tendency equation terms, and are large in every scale. This suggests that large fluxes of kinetic energy occur between subgrid scales $n>24$ and scales $n\leqslant 24$. The spectral indices where large tendencies of total kinetic energy occur, and the variation with pressure of these indices, agree with theoretical studies of baroclinic and barotropic–baroclinic instability.

The total nonlinear transfer of kinetic energy reveals sources of kinetic energy in scales $4\leqslant n\leqslant 10$, $13\leqslant n\leqslant 15$, $n=18$ and $n=23$, with scales $n\leqslant 3$ gaining kinetic energy in the fashion of the zonal flow in l domain calculations (Fourier expansion at latitude circules). The peak sources are at $n=7$ and $n=9$. The isolated source at $n=18$ is strong and may be due to the ITCZ, which can be described by expansion indices $n\approx 18$ and $l\approx 0$. The presence of kinetic energy sources in scales $15\leqslant n\leqslant 24$, and the slope of kinetic energy with scale there, suggest that motion in these scales cannot be described by two-dimensional random isotropic turbulence theory, insofar as data accuracy is accepted.

Isolation of the contributions of nonlinear interaction of motion in scale ranges $0\leqslant n\leqslant 6$, $7\leqslant n\leqslant 14$ and $15\leqslant n\leqslant 24$ proved interesting, and this approach is suggested as a means of diagnosing the impact of dissipation and heating parameterizations upon all scales of motion in models of the atmosphere. The results showed that nonlinear horizontal transfers of kinetic energy occur by a complex set of interactions. Some general observations are listed at the end of Section 4.

Acknowledgments. This work was undertaken while I was on leave from the Atmospheric Environment Service, Environment Canada. I express my gratitude to Prof. Ferdinand Baer of the University of Michigan for his guidance during the course of this research, and for providing support under National Science Foundation Grant OCD73-06436-AO2. I am indebted to the National Center for Atmospheric Research, sponsored by National Science Foundation, for granting computer time and the services of Roy Jenne and Dennis Joseph of the Atmospheric Technology Division. Jim Sterken of the University of Michigan handled much of the I/O programming.

The material shown here is taken from my Ph.D. dissertation, submitted to the Department of Atmospheric Science, Colorado State University, and appears in Report 011128-1-T of the Department of Atmospheric and Oceanic Science, University of Michigan.

REFERENCES

Baer, F., 1972: An alternate scale representation of atmospheric energy spectra. *J. Atmos. Sci.*, **29**, 649–664.

Bedient, H. A., W. G. Collins and G. Dent, 1967: An operational tropical analysis system. *Mon. Wea. Rev.*, **95**, 942–949.

Bourke, W., 1974: A multi-level spectral model. I. Formulation and hemispheric integrations. *Mon. Wea. Rev.*, **102**, 687–701.

Brown, J. A., 1969a: A numerical investigation of hydrodynamic instability and energy conversions in the quasi-geostrophic atmosphere: Part I. *J. Atmos. Sci.*, **26**, 352–365.

——, 1969b: A numerical investigation of hydrodynamic instability and energy conversions in the quasi-geostrophic atmosphere: Part II. *J. Atmos. Sci.*, **26**, 366–375.

Burrows, W. R., 1974: Merging of data on NMC. octagonal and Mercator grids for hemispheric analysis. *Mon. Wea. Rev.*, **102**, 76–81.

Charney, J. G., 1971: Geostrophic turbulence. *J. Atmos. Sci.*, **28**, 1087–1095.

Eliasen, E., B. Machenhauer, and E. Rasmussen, 1970: On a numerical method for integration of the hydrodynamical equations with a spectral representation of the horizontal fields. Rept. No. 2, Copenhagen University, Institute for Theoretical Meteorology, 35 pp.

Ellsaesser, H. W., 1966: Expansion of hemispheric meteorological data in antisymmetric surface spherical harmonic (Laplace) series. *J. Appl. Meteor.*, **5**, 263–276.

Kanamitsu, M., T. N. Krishnamurti and C. Depradine, 1972: On scale interactions in the tropics during northern summer. *J. Atmos. Sci.*, **29**, 698–706.

Kuo, H. L., 1953: The stability properties and structure of disturbances in a baroclinic atmosphere. *J. Meteor.*, **10**, 235–243.

Machenhauer, B., and R. Daley, 1972: A baroclinic primitive equation model with a spectral representation in three dimensions. Rept. No. 4, Copenhagen University, Institute for Theoretical Meteorology, 63 pp.

——, and E. Rasmussen, 1972: On the integration of the spectral hydrodynamical equations by a transform method. Rept. No. 3, Copenhagen University, Institute for Theoretical Meteorology, 44 pp.

Miyakoda, K., R. F. Strickler, C. J. Nappo, P. L. Baker and G. D. Hembree, 1971: The effect of horizontal grid resolution in an atmospheric circulation model. *J. Atmos. Sci.*, **28**, 481–499.

Orszâg, S. A., 1970: Transform method for the calculation of vector-coupled sums: Application to the spectral form of the vorticity equation. *J. Atmos. Sci.*, **27**, 890–895.

Platzman, G. W., 1960: The spectral form of the vorticity equation. *J. Meteor.*, **17**, 635–644.

Unauthenticated | Downloaded 01/19/22 11:11 AM UTC

Saltzman, B., 1970: Large-scale atmospheric energetics in the wavenumber domain. *Rev. Geophys.*, **19**, 195–204.

——, and A. Fleisher, 1962: Spectral statististics of the wind at 500 mb. *J. Atmos. Sci.*, **19**, 195–204.

Shuman, F. G., and J. B. Hovermale, 1968: An operational six-layer primitive equation model. *J. Appl. Meteor.*, **7**, 525–546.

Simmonds, I., 1974: Spectral representation of horizontal wind in numerical models of the atmosphere. *J. Appl. Meteor.*, **13**, 221–226.

Wellck, R. C., A. Kasahara, W. M. Washington and G. DeSanto, 1971: Effect of horizontal resolution in a finite-difference model of the general circulation. *Mon. Wea. Rev.*, **99**, 673–685.

Wiin-Nielsen, A. C., 1972: A study of power laws in the atmospheric kinetic energy spectrum using spherical harmonic functions. *Meteor. Ann.*, **6**, 107–124.

Unauthenticated | Downloaded 01/19/22 11:11 AM UTC